The 12th International Conference of
International Association for Computer Methods and Advances in Geomechanics (IACMAG)
1-6 October, 2008
Goa, India

Computation of Soil Penetration at Finite Strains by Using Arbitrary Lagrangian-Eulerian Methods

D. Aubram, F. Rackwitz and S. A. Savidis
Soil Mechanics and Geotechnical Engineering Division, Technical University of Berlin, Germany

Keywords: Arbitrary Lagrangian-Eulerian, large deformation, sand, penetration, pile

ABSTRACT: The paper presents a framework for the numerical simulation of soil penetration at finite strains based on the Arbitrary Lagrangian-Eulerian (ALE) finite element method. By applying an operator-split to the governing ALE equations, the usual computation with finite elements, which is then referred to as the Lagrangian step, is followed by a mesh regularisation step which should reduce the element distortions occurred during the calculation. Thereafter, the state variables are remapped onto the updated mesh allowing for the convection of the material. When combining the ALE approach with advanced stress and density dependent constitutive equations for sand, managing this convection step is an important task. This paper presents a couple of numerical schemes and results of numerical examples will illustrate the advantages of the ALE framework in comparison to the classical Lagrangian formulation.

1 Introduction

Measurements in the course of the large geotechnical projects at the Potsdamer Platz and the new Central Station in Berlin show that the deformation of the walls of deep excavation pits during the construction was generally larger then that predicted by the numerical simulations. A typical finite element simulation starts "after" the construction, i.e. with the structure wished-in-place and in an assumed material state. However, Savidis and Mittag (1999) and Triantafyllidis (1998) concluded that the construction process of the anchoring piles has a considerable impact on the surrounding soil and thus constitutes an important factor. In this context, the penetration of piles into sand and its computation is confirmed as one of the most complex problems in geomechanics, because it causes large strains in the vicinity of the pile tip, the soil exhibits strong non-linear behaviour, the contact conditions between pile and soil are complex, and both the free surfaces and the boundaries at material interfaces do move.

Classical Lagrangian and Eulerian versions of the finite element method are not suitable for a realistic simulation of pile penetration. In the Lagrangian formulation, which is standard in solid mechanics, the mesh moves along with the material so that excessive element distortions may occur. This often leads to unstable and inaccurate numerical analyses, or even to termination of the calculation (Armero and Love, 2003). In the Eulerian formulation, which is more common in fluid dynamics, the discretised domain is fixed in space. Its weakness relates to the difficulties in representing free surfaces and moving boundaries, inasmuch as the computational grid and the material are uncoupled (Armero and Love, 2003).

The Arbitrary Lagrangian-Eulerian (ALE) formulation (Hirt et al., 1974; Donea et al., 2004) succeeds in combining the advantages of classical Lagrangian and Eulerian viewpoints. Kinematics of a body is described with reference to an almost arbitrary time-dependent domain that is uncoupled from the material (Lagrange) and the spatial (Euler) configurations. When applying the ALE formulation to the finite element method, the element mesh is chosen as the reference domain. Due to the relative motion between the element mesh and the material, analogous to the Eulerian formulation convective terms enter the governing ALE equations. The treatment of these terms plays a crucial role in the numerical implementation, especially for complex path-dependent materials such as in soil mechanics. Benson (1989) proposes a split of the ALE operator into three steps, so as to allow the use of simple algorithms and the upgrade of standard Lagrangian finite element codes.

During the last decades the ALE methods became a widely-used analysis tool for metal forming processes and free surface flows. The application of ALE to geomechanics is on the upswing and mostly incorporate simple constitutive equations to model the nonlinear soil behaviour (Di et al., 2007; Nazem et al. 2007). However, the incorporation of an advanced constitutive equations within the numerical simulation of soil penetration is as much important as the appropriate discretisation of the domain in order to produce realistic results.

The paper proceeds as follows. Section 2 presents the derivation of the fundamental ALE operator from the kinematics of a material body relative to a reference domain by applying a modern geometric language. In section 3, the mechanical behaviour of sandy soil under monotonic and cyclic loads is briefly reviewed. Section 4 illustrates the calculation steps and the implementation requirements of the ALE framework in the context of the finite element method. Finally, initial results of ALE simulations are compared to classical Lagrangian solutions in section 5.

2 Arbitrary Lagrangian-Eulerian formulation

The following section introduces some basic results concerning the kinematics of a material body from the Lagrangian, Eulerian and ALE viewpoints and it provides a formulation of the fundamental ALE operator. A common choice in mechanics is to use the Euclidean three-space as the background. However, differential geometry has been found to be the appropriate language to present continuum mechanics in a more general framework (Bishop and Goldberg, 1968; Marsden and Hughes, 1994). Accepting this intention, the notation within the paper largely follows Marsden and Hughes (1994), by applying the ALE-terminology used by Donea et al. (2004) in particular. For a comprehensive overview of ALE methods in mechanics, see Donea et al. (2004) and the references therein.

2.1 Kinematics relative to an arbitrary time-dependent reference domain

Let M denote a sufficiently differentiable material manifold. A part $B \subseteq M$, consisting of open sets of particles $p \in B$, is referred to as material body. During its motion $\kappa_t : B \to S$, B occupies time dependent placements $D \subseteq S$ in the ambient space S, which is assumed to be Riemannian (Marsden and Hughes, 1994). At fixed time t_0, $D_0 = \kappa_0(B)$ and $q_0 = \kappa_0(p)$ denote the initial placement of the body and the initial position of p, respectively (Figure 1).

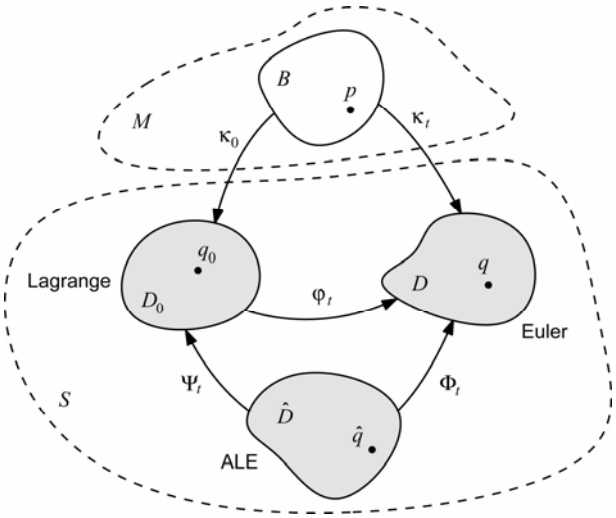

Figure 1. Arbitrary Lagrangian-Eulerian (ALE) formulation: material body *B*, part of the material manifold *M*, initial placement D_0, current placement D and reference domain $\hat{D}$ (all part of the Riemannian manifold *S*, the ambient space), related mappings κ_0, κ_t, φ_t, Ψ_t and Φ_t.

The local coordinates $X(q_0) = \{X^1, X^2, X^3\} = \{X^I\}$ of a chart (U_0, X), in which $U_0(q_0) \subseteq D_0$ is an open neighbourhood of q_0, enable measurement on the body. If the meaning is clear, the picture $X(q_0)$ in the chart is identified with the particle respectively its initial position. Since S is differentiable, $\partial/\partial X^I \in T_{q_0} D_0$ forms a base and $dX^I \in T^*_{q_0} D_0$ its dual at q_0. $T_{q_0} D_0$ and $T^*_{q_0} D_0$ denote the tangent space and co-tangent space, respectively. The definition of counterparts on the current placement $D = \kappa_t(B)$ is straightforward: (U, x) denotes a local chart and $\partial/\partial x^i \in T_q D$ is the base at $q = \kappa_t(p)$. As κ_t is meant as an embedding, chart transitions between X and x should be compatible.

A common convention is to use upper case roman letters as symbols to denote coordinates, vectors and tensors expressed in the Lagrangian formulation, and lower case roman letters for the Eulerian formulation. Alternatively, one can add a zero subscript in the Lagrangian formulation to distinguish entities from the Eulerian formulation.

The particle flow $q = \varphi_t(q_0), \exists \varphi_t^{-1}$ in the ambient space, where $\varphi_0(q_0) = q_0$, communicates the relocation from D_0 to D at every time *t*. Defining $x^i(q) = \varphi_t^i(q_0) := x^i \circ \varphi_t \circ X^{-1}$ as a function of the motion φ_t, in which $\circ$ denotes the composition of maps, then

$$\boldsymbol{V}_t = \left.\frac{\partial \varphi_t^i}{\partial t}\right|_{q_0} \frac{\partial}{\partial x^i} =: V_t^i(q_0)\frac{\partial}{\partial x^i}(q) \tag{1}$$

is the particle velocity field at *t* —written as the Lagrangian velocity field. Switching the reference points gives the spatial or Eulerian velocity field: $\boldsymbol{v}_t = \boldsymbol{V}_t \circ \varphi_t^{-1} =: v_t^i \, \partial/\partial x^i$. $\boldsymbol{v}_t(q) : D \to TD$ is a proper velocity field on *D*, whereas $\boldsymbol{V}_t$ is not (Marsden and Hughes, 1994). $TD = \bigcup_{q \in D} T_q D$ denotes the tangent bundle of *D*.

Within the description of a physical field, at a spatial point the physical quantity $\beta(q,t)$ can be observed —here β stands for an arbitrary tensor-valued function of (q,t), i.e. a scalar, vector or tensor field on *D*. By noting that $q = \varphi(q_0, t)$ is also understand to be the current position of a particle, the same physical field can be written as $\beta_0(q_0,t)$. Depending on whether q_0 or q serve as the independent variables, $\beta_0(q_0,t) = \beta \circ \varphi_t$ and $\beta(q,t)$ are referred to as the Lagrangian (or material) and the Eulerian formulation of the field, respectively —for simplicity, the difference between β and $\beta \circ x^{-1}$ respectively β_0 and $\beta_0 \circ X^{-1}$ is dropped throughout the paper. The material time derivative is an important link between the Lagrangian and the Eulerian formulation:

$$\frac{D\beta}{Dt}(q,t) := \left.\frac{\partial \beta_0}{\partial t}\right|_{q_0} \circ \varphi_t^{-1} = \left.\frac{\partial \beta}{\partial t}\right|_q + \nabla_{\boldsymbol{v}}\beta \qquad = \Upsilon(q,t) \ . \tag{2}$$

Therein, $\nabla_{\boldsymbol{v}}\beta(q,t)$ is the covariant derivative of β along the Eulerian velocity field $\boldsymbol{v}$ (Marsden and Hughes, 1994) and $\Upsilon(q,t)$ is a source term accounting for some corresponding response functions, e.g. a constitutive equation.

In the ALE framework, an arbitrary reference domain $\hat{D} \subseteq S$ is introduced, presuming the map $\hat{D} \to B$ to be invertible. The reference domain consists of open sets of reference points $\hat{q}$ and generally depends on time (Figure 1). By using the charts with local coordinates χ^μ assigned to neighbourhoods of the $\hat{q}$, a vector basis $\partial/\partial\chi^\mu \in T_{\hat{q}}\hat{D}$ at the reference points is defined. As a general convention, quantities related to the reference domain or to the ALE formulation are denoted by lower case greek letters or by a superposed caret.

The referential map $\Psi_t : \hat{D} \to D_0$ and the relative map $\Phi_t : \hat{D} \to D$ satisfy the conditions $\Psi_0 \equiv \Phi_0$ at $t = t_0$ and $q(t) = \varphi_t(q_0) = \Phi_t \circ \Psi_t(q_0)$ (Figure 1). Defining coordinate functions $\Phi_t^i(\hat{q}) := x^i \circ \Phi_t \circ \chi^{-1}$ and $(\Psi_t^{-1})^\mu(q_0) := \chi^\mu \circ \Psi_t^{-1} \circ X^{-1}$, it seems reasonable to introduce additional velocity fields:

$$\left(\left.\frac{\partial (\Psi_t^{-1})^\mu}{\partial t}\right|_{q_0} \circ \Psi_t\right)\frac{\partial}{\partial \chi^\mu} =: \upsilon_t^\mu(\hat{q})\frac{\partial}{\partial \chi^\mu} \qquad \text{and} \qquad \left(\left.\frac{\partial \Phi_t^i}{\partial t}\right|_{\hat{q}} \circ \Phi_t^{-1}\right)\frac{\partial}{\partial x^i} =: w_t^i(q)\frac{\partial}{\partial x^i} \tag{3}$$

are the referential velocity field on $\hat{D}$ and the grid or mesh velocity on *D*, respectively. A substitution of $\varphi_t = \Phi_t \circ \Psi_t$ for the Eulerian velocity $\boldsymbol{v}_t$ yields

$$v_t^i(q) = w_t^i(q) + \left(\left(\frac{\partial \Phi_t^i}{\partial \chi^\mu}\upsilon_t^\mu\right) \circ \Phi_t^{-1}\right)(q) =: w_t^i(q) + c_t^i(q) \qquad \text{or} \qquad \boldsymbol{c}_t = \boldsymbol{v}_t - \boldsymbol{w}_t \ . \tag{4}$$

The bracket term is of fundamental importance within the ALE formulation. It denotes the components of the convective velocity field $\boldsymbol{c}_t$. From Equation (4) and the definition given in Marsden and Hughes (1994), conclude that $\boldsymbol{c}_t$ is the pushforward of the referential velocity field $\boldsymbol{v}_t$ over Φ_t:

$$\boldsymbol{c}_t = T\Phi_t \circ \boldsymbol{v}_t \circ \Phi_t^{-1} = \Phi_{t*}\boldsymbol{v}_t, \tag{5}$$

in which the components of the tangent map are given by $(T\Phi_t)^i{}_\mu = \partial\Phi_t^i / \partial\chi^\mu$.

2.2 The ALE operator

Through $\hat{D}$, Φ_t and Ψ_t the picture of a physical quantity in the reference domain is defined by $\hat{\beta} = \beta \circ \Phi_t = \beta \circ \varphi_t \circ \Psi_t = \beta_0 \circ \Psi_t$. That is, if $\beta : D \to TD$ is vector-valued, then $\hat{\beta} : \hat{D} \to TD$ is a vector field over Φ_t. Let $\gamma_k{}^i{}_j$ denote the coefficients of the affine connection ∇ on D. Then Φ_t induces a connection ∇^* on $\hat{D}$ satisfying

$$\nabla^*_{\boldsymbol{v}} \hat{\beta}\,(\hat{q},t) = \left(\frac{\partial \hat{\beta}^i}{\partial \chi^\mu} \upsilon_t^\mu + \hat{\beta}^j \upsilon_t^\mu \gamma_k{}^i{}_j \frac{\partial \Phi_t^k}{\partial \chi^\mu} \right) \frac{\partial}{\partial x^i} = \nabla_{(\boldsymbol{c}\circ\Phi)}\beta \tag{6}$$

and having coefficients $\gamma_k{}^i{}_\mu := \gamma_k{}^i{}_j (T\Phi_t)^j{}_\mu$ (Bishop and Goldberg, 1968). The material time derivative of $\hat{\beta}$ concerning $\hat{q}$ then reads

$$\frac{D\hat{\beta}}{Dt}(\hat{q},t) = \left.\frac{\partial \hat{\beta}}{\partial t}\right|_{\hat{q}} + \nabla^*_{\boldsymbol{v}}\hat{\beta} = \left.\frac{\partial \hat{\beta}}{\partial t}\right|_{\hat{q}} + \nabla_{(\boldsymbol{c}\circ\Phi)}\beta\ . \tag{7}$$

By noting that $D/Dt\ \hat{\beta}(\Psi_t^{-1}(q_0),t) = \partial\beta_0/\partial t\big|_{q_0}$, one finally obtains the Arbitrary Lagrangian-Eulerian operator (Donea et al., 2004, eq. 27) extended to Riemannian manifolds:

$$\left.\frac{\partial \beta_0}{\partial t}\right|_{q_0} \circ \Psi_t = \left.\frac{\partial \hat{\beta}}{\partial t}\right|_{\hat{q}} + \nabla_{(\boldsymbol{c}\circ\Phi)}\beta \qquad = \hat{\Upsilon}(\hat{q},t)\ . \tag{8}$$

in which $\hat{\Upsilon}(\hat{q},t)$ again is a source term. Equation (8) states that the material time derivative of a quantity β consists of a local time derivative at fixed reference point $\hat{q}$ plus a convective term due to the relative motion between the body and the reference domain as measured from a fixed spatial point q.

3 Macroscopic mechanical behaviour of sand and constitutive modeling

During soil penetration, the soil may take up multiple material states. The loading paths are often complex, deformation is highly variable in space and time, and the drainage conditions may vary. The section that follows briefly introduces the phenomenology of the macroscopic mechanical behaviour of sand and the use of constitutive equations developed for its mathematical set-up. For further information, see Savidis et al. (2007) and the references therein.

3.1 Mechanical characteristics of sand

From the viewpoint of kinematics, strain can be decomposed into pure volumetric and deviatoric parts. However, from the viewpoint of constitutive modeling, this is not possible for sand because its volume changes due to shear loading. This so-called dilative behaviour depends on both the stress state and the density state. Figure 2 shows the dilative response of Toyoura sand with various initial relative densities D_r under the same initial state of stress p_0' and under drained triaxial compression. Note that under triaxial conditions, the axial strain ε_1 is a shear strain measure. A specimen of sand with a sufficient low initial density contracts monotonically (Figure 2a) and leads to a monotonically increasing shear stress (Figure 2b). If the initial density is sufficient high, sand

shows little contraction at small shear strains. Under continued shear loading, the sand passes a transformation state, at which the response changes from contraction to dilation and the sand continues to dilate until a residual state is reached (Figure 2a). At sufficiently high initial densities, the deviatoric stress $q = \sigma_1 - \sigma_3$ increases until it reaches a peak value which coincides with the zero volume change in the strain-plane. Analogous results can be obtained by a variation of the confining pressure p_0' at the same initial density. Thus, both the stress state and the density state have to be accounted for to specify the material state of sand.

Sand is a multiphase medium and, therefore, the mechanical behaviour also depends on the drainage condition. If the initial density is sufficiently low under undrained conditions, the effective mean normal stress and the shear strength drop dramatically, due to the loss of particle contacts. This is of utmost importance under cyclic loading conditions, because the loading direction changes faster than the soil consolidates due to the changed loading conditions. Depending on the confining pressure and on the loading amplitude, an initially loose sand may be subjected to a complete loss of shear resistance and sustains large shear deformations, due to gradually increasing excessive pore water pressure. This phenomenon is also referred to as liquefaction.

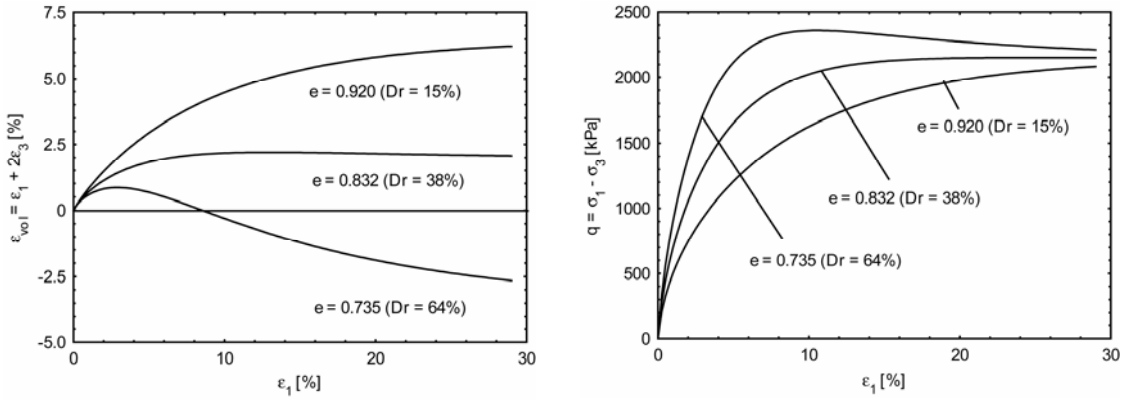

(a) (b)

Figure 2. Dilative behaviour of sand under drained triaxial compression: dependency on the density state. Toyoura sand, p_0' =1000 kPa.

3.2 Constitutive Equations

In the last decades, a large number of constitutive equations for soil has been developed, so it is difficult for the user to make an appropriate choice. However, only a few of these constitutive models are able to simulate the mechanical behaviour of sand under complex loading paths over a wide range of densities and stress states by using just one set of parameters. The most popular fall into the groups of elastoplastic or hyperelastoplastic models and hypoplastic models.

The finite strain formulation of hyperelastoplastic soil models is an exception. Mostly, strains are assumed to be small and the elastic and plastic strains are decomposed additively. A crucial point is that hyperelastoplastic constitutive equations require the information of deformation as a whole, i.e. the deformation occurred from the initial to the current placement. By contrast, the class of hypoplastic models comprehends constitutive equations of the rate-type, that is, they are expressed in terms of stress and strain rates together with a specification for finite strains (Truesdell and Noll, 2004). In geomechanics, hypoplastic models were firstly developed by Gudehus and Kolymbas (1979). By introducing a so-called intergranular strain, Niemunis and Herle (1997) have extended a model for sand of the general form

$$\overset{\Delta}{\boldsymbol{\sigma}} = \boldsymbol{h}(\boldsymbol{\sigma}, \boldsymbol{d}, e) \tag{9}$$

for cyclic loading conditions, in which $\boldsymbol{\sigma}$ is the Cauchy stress, $\overset{\Delta}{\boldsymbol{\sigma}}$ denotes an objective stress rate, $\boldsymbol{d}$ is the spatial (Eulerian) rate of deformation tensor and e denotes the void ratio. Recalling that the ALE formulation covers large deformations and an initial placement of the body is usually unavailable, it seems reasonable to implement a rate-type model for the simulation of pile penetration. In fact, this decision can be seen as a standard choice in the ALE community.

4 Finite Element Implementation

4.1 Operator-split

The handling of the convective term in Equation (8), which emerges from the time-dependency of the reference domain, plays a fundamental role in the ALE framework. This is of particular importance if path-dependent materials such as soil are involved. The needed algorithms are usually simpler and more robust than algorithms for the fully coupled problem, if an operator-split (Benson, 1989) of the governing equations is applied. Another advantage of the operator-split growth from the facility to upgrade existing Lagrangian finite element programmes. Applying the operator-split to Equation (8) yields

$$\left.\frac{\partial \beta_0}{\partial t}\right|_{q_0} = \Upsilon_0(q_0, t) \qquad \text{and} \qquad \left.\frac{\partial \hat{\beta}}{\partial t}\right|_{\hat{q}} + \nabla_{(c \circ \Phi)} \beta = 0 \ . \tag{10}$$

The solution of the operator-split ALE methods then proceeds in three steps. In the first step, the parabolic equation $(10)_1$ is solved. Since there is no difference to classical approaches in solid mechanics using Lagrangian finite element codes, this step is referred to as the Lagrangian step. Non-linear constitutive equations can be incorporated in a well-established way. In the Lagrangian step, heavy element distortion may occur, especially during the simulation of soil penetration. The intention of the second step then is to reduce these distortions by applying suitable rezoning or mesh regularisation techniques. In the last phase of the calculation, which is referred to as the convection step, the state variables respectively the values of the physical fields β of the Lagrangian step are mapped to the updated mesh concerning equation $(10)_2$.

4.2 Algorithms for mesh regularisation

The quality of the finite element mesh is important for realistic and accurate numerical simulations. If the mesh topology is kept fixed during the calculation, then some activity which avoids highly squeezed and distorted elements is referred to as mesh regularisation, while eliminating crowding of nodes in regions of secondary interest calls for mesh adaptation. By applying the operator-split ALE framework to the finite element method, it becomes possible for the user to optimise the mesh after the Lagrangian step of calculations.

A distinction is drawn between the nodes to be moved in order to increase the mesh quality. For internal nodes, there is a large amount of algorithms available that regularise the mesh. Unfortunately, many of these methods only succeed if the boundaries are convex. If the boundaries are non-convex, such as the soil regions around a pile tip at deep penetration, internal nodes as a result may run outside and the mesh gets folded. Algorithms which overcome mesh folding, even in unstructured meshes, are, for example, Winslow smoothing (Knupp, 1999), Giuliani smoothing (Giuliani, 1982) and energy-based methods (Braess and Wriggers, 2000).

As shown by Braess and Wriggers (2000), the benefit of appropriate regularisation schemes is limited if the location of the boundary nodes remains unchanged. In two-dimensional meshes, boundaries can simply be regularised by averaging procedures in order to improve the quality of the complete mesh considerably (Aymone 2004). Corner nodes of the domain are not moved, because they define the shape of the domain.

An important measure for the squeeze and distortion of triangular elements is the ratio of radii of the circumcircle r_{out} and the incircle r_{in}, respectively. The ratio is $r_{\text{out}} / r_{\text{in}} = 2.0$ for equilateral triangles and approaches infinity if the element degenerates. From this, Braess and Wriggers (2000) propose the potential

$$W = \sum_{elements} \omega = \sum_{elements} \frac{r_{\text{out}}}{r_0} \left(\frac{r_{\text{out}}}{r_{\text{in}}} \right)^3 = \text{Min} \ , \tag{11}$$

which has to be minimised. $r_0 = 1.0$ is a reference radius. It is sufficient to reach a local minimum of the potential in terms of element patches enclosing a single internal node. Therefore, the sum in Equation (11) is over the number of elements in the patch and standard minimisation algorithms, such as Newton's method, can be applied to obtain a location $\boldsymbol{x}_{\text{int}}$ of the internal node that regularises the element patch.

4.3 Convection of the state variables

In the convection step, the values of the field β calculated in the Lagrangian step are mapped on the updated (regularised) mesh, according to Equation $(10)_2$. Note that on the boundary of the domain and on the material

interfaces, the normal components of the relative velocity between the material and the mesh are zero. The main challenge in solving Equation $(10)_2$ is found in the determination of the gradient $\nabla_{(c\circ\Phi)}\beta$, because variables are discontinuous across the element edges as they are evaluated at the Gauss points and not at the element nodes. In the ALE community, two approaches are established. The first strategy is to obtain a smooth β-field with a smooth gradient and then applying Lax-Wendroff or Taylor-Galerkin schemes (Rodríguez-Ferran et al., 1998). In the second approach, cells where β is constant are constructed for each Gauss point, and then Godunov-type algorithms are performed. By applying the latter, Rodríguez-Ferran et al. (1998) propose the following formula for a triangular mesh that has to be evaluated for each element:

$$\beta^{n+1} = \beta^{\mathrm{L}} - \frac{\Delta t}{2A}\sum_{i=1}^{3} f_{S_i}\left(\beta_{S_i} - \beta^{\mathrm{L}}\right)\left(1-\mathrm{sign}(f_{S_i})\right). \tag{12}$$

Herein, β^{L} and β^{n+1} denote the value of the field after performing the Lagrangian step and at the end of the time increment, respectively, β_{S_i} is the value of the field in the neighbouring element owning the shared element edge S_i and $\mathrm{sign}(\cdot)$ is the sign function. $f_{S_i} = \int_S \left(\boldsymbol{n}^* \cdot \boldsymbol{c}\right) dS_i$ is the flux of the convective velocity field across the element edge S_i, with $\boldsymbol{n}^*$ as the unit normal field on the element boundary $\mathcal{S}$.

5 Numerical examples

By following the operator-split ALE framework described in the previous sections, the authors have upgrade the commercial implicit Lagrangian finite element code ANSYS (Ansys, 2004) in order to analyse finite strain soil penetration problems and in particular pile penetration numerically. The background code provides several user interfaces for customisation. Users can implement extra constitutive equations and element types or they can benefit from the provided routines for accessing the database.

Kinematics of pile penetration is characterised by non-convex soil regions around the pile tip during penetration that suffer from severe element distortion in a pure Lagrangian finite element simulation. In this section, examples will be presented which highlight the advantages and drawbacks of three different algorithms for mesh regularisation that have been implemented to overcome this problem: barycentric regularisation (Aymone, 2004), Giuliani rezoning (Giuliani, 1982) and energy-based regularisation (Braess and Wriggers, 2000).

5.1 Coining test

The coining test is a common problem in the metal forming community. Therein, a rigid die is punched into an elastic plate (Figure 3). The finite element model takes advantage of axial symmetry by fixing the left nodes in horizontal direction. The lower boundary nodes are fixed in the vertical direction. Slippery contact between the die and the target material reduces loading to a simple vertical displacement of the interface nodes. Except for the four corner nodes and the node at the lower right corner of the die, all nodes are available for mesh regularisation.

Figure 3a shows the edges of the undeformed structure together with the deformed mesh at the stage of 50% indentation resulting from a pure Lagrangian calculation, i.e. without performing mesh regularisation. Even directly under the lower right corner of the die the distortion of the mesh is moderate (circled area). However, if a higher mesh quality is intended, energy-based regularisation seems to be appropriate, as shown in Figure 3b. On the other hand, the application of improper algorithms may reduce the mesh quality, as shown in Figures 3c and 3d for Giuliani rezoning and barycentric regularisation, respectively. The mesh distortion after barycentric regularisation is even higher than after Giuliani rezoning.

In Figures 3b-3d, the algorithm for regularisation of the boundary nodes is a simple averaging procedure which places a node in the center of its two neighbours on a parabola (Aymone, 2004).

5.2 Back extrusion problem

The boundary conditions of a back extrusion problem (Figure 4) and these of a coining test are comparable. The difference is the suppression of the horizontal displacements of all vertical aligned boundary nodes in the case of the back extrusion problem. Figure 4 top shows the edges of the undeformed structure together with the deformed element mesh at 30% indentation. The results of the calculation using Giuliani rezoning is shown on the left hand side, whereas the right hand side results from the energy-based algorithm according to Equation (11). At 50% indentation and applying Giuliani rezoning, elements around the corner of the die are extremely squeezed. The area of one element even vanishes, which inhibits the convergence of the solution at higher indentation.

When using energy-based mesh regularisation, the squeeze and distortion of elements is moderate at 50% indentation, even directly below the die. However, at higher indentation, the rigid mesh topology together with the simplified local form of Equation (11), i.e. to achieve a local instead of a global minimum, limits gains of mesh quality. Calculation terminates at indentations of more than 71%. Only complete remeshing would eliminate element degeneration in order to ensure a convergent solution.

5.3 Penetration of a rigid pile

Figure 5 illustrates simulation results of the penetration of a rigid pile into elastic soil material, assuming slippery contact conditions between the pile and the soil. The finite element mesh after a Lagrangian calculation is shown on the left. Elements below the semispherical pile tip are heavily squeezed. The area of the first element row even vanishes, as brought out by the detail. On the other hand, elements next to the pile at the free surface are stretched, thus reducing the density of nodes and the accuracy of the results in regions of a strong solution gradient.

Figure 5 on the right shows the results of the simulation by using the ALE finite element method. The mesh is obtained through an energy-based regularisation of the internal nodes and a simple averaging procedure for the boundary nodes. From the detail, it can be seen that the problematic regions discussed benefit from the implemented algorithms to increase the mesh quality after the Lagrangian calculation step. Squeezing of elements below the pile tip is much reduced. The averaging procedure for the free surface nodes naturally avoids large stretching of the associated elements and maintains the initial density of nodes lateral to the pile. Compared to barycentric regularisation and Giuliani rezoning, the energy-based scheme yields the best results.

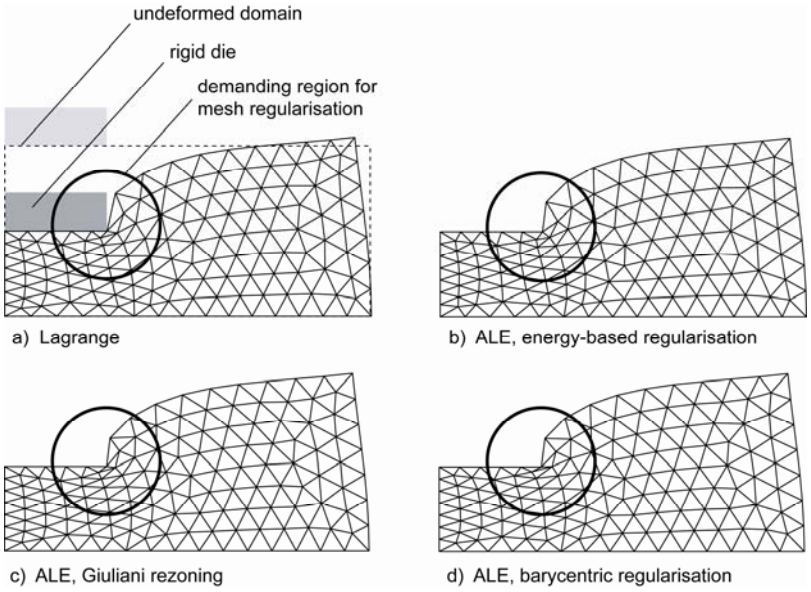

Figure 3. Comparison of different mesh smoothing schemes applied to the numerical simulation of a coining test at the stage of 50 % indentation. (a) Lagrangian mesh and ALE mesh with (b) energy-based regularisation, (c) Giuliani rezoning, (d) barycentric regularisation.

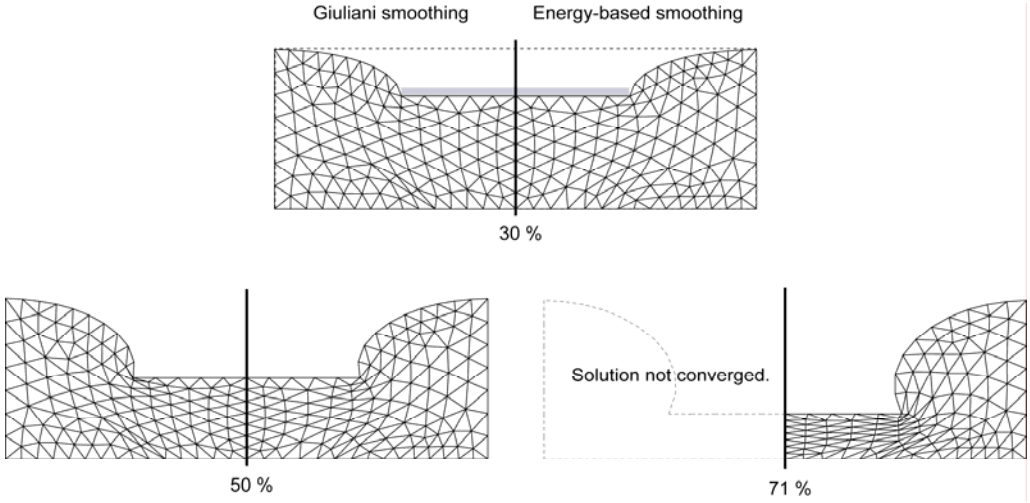

Figure 4. Comparison of Giuliani rezoning and energy-based regularisation applied to the numerical simulation of a back extrusion problem at different indentations.

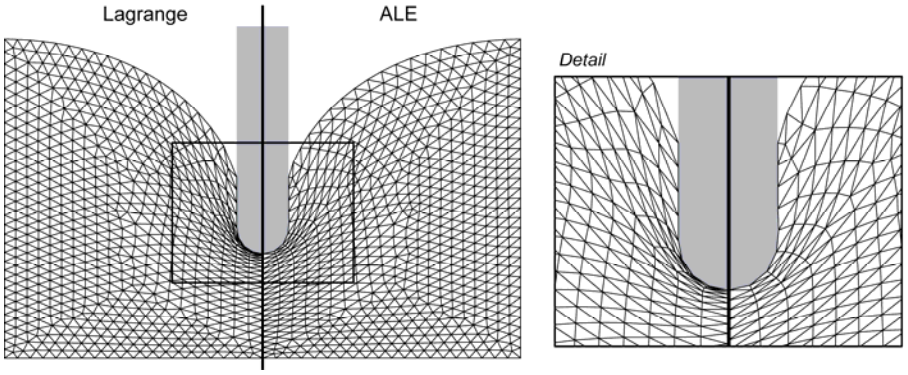

Figure 5. Numerical simulation of the penetration of a smooth rigid pile into elastic material. left: Lagrangian mesh, right: ALE mesh with energy-based regularisation.

6 Summary

A framework for the simulation of soil penetration at finite strains based on the Arbitrary Lagrangian-Eulerian (ALE) finite element method has been presented. For the numerical implementation, an operator-split has been applied in order to enforce simpler equations and to achieve the possibility to update an existing Lagrangian finite element code. Three different mesh regularisation schemes have been implemented and applied to different boundary value problems. It has been shown by the numerical simulation of a coining test, a back extrusion problem and pile penetration, that handling non-convex mesh regions plays a crucial role.

The results presented are based on the assumption of an elastic material. Further developments should incorporate an advanced hypoplastic constitutive equation, which is able to model the surrounding soil, especially sand, in context of ALE more realistically. In this case, the numerical implementation is more complicated and the choice of the numerical algorithms plays an important role, since convective terms affect the update of the state variables of the governing equation.

7 Acknowledgements

The presented research work has been carried out with the financial support from DFG (German Research Foundation), grant SA 310/21-1, which is gratefully acknowledged.

8 References

ANSYS 2004. *Guide to ANSYS User Programmable Features – ANSYS Release 8.1*, No. 001975, ANSYS, Inc.

Aymone J.L.F. 2004. Mesh motion techniques for the ALE formulation in 3D large deformation problems, *International Journal for Numerical Methods in Engineering*, **59**(14), 1879-1908.

Armero F., Love E. 2003. An arbitrary lagrangian-eulerian finite element method for finite strain plasticity, *International Journal for Numerical Methods in Engineering*, **57**(4), 471-508.

Benson D.J. 1989. An efficient, accurate, simple ALE method for nonlinear finite element programs, *Computer Methods in Applied Mechanics and Engineering*, **72**(3), 305-350.

Bishop R.L., Goldberg S.I. 1968. *Tensor Analysis on Manifolds*, The Macmillan Company, New York (USA).

Braess H., Wriggers P. 2000. Arbitrary lagrangian eulerian finite element analysis of free surface flow, *Computer Methods in Applied Mechanics and Engineering*, **190**(1), 95-109.

Di Y., Yang J., Sato T. 2007. An operator-split ALE model for large deformation analysis of geomaterials, *International Journal for Numerical and Analytical Methods in Geomechanics*, **31**(12), 1375-1399.

Donea J., Huerta A., Ponthot J.-P., Rodríguez-Ferran A. 2004. Arbitrary lagrangian-eulerian methods, *Encyclopedia of Computational Mechanics*, John Wiley & Sons, New York (USA).

Giuliani P.M. 1982. An algorithm for continuous rezoning of the hydrodynamic grid in arbitrary lagrangian-eulerian computer codes, *Nuclear Engineering and Design*, **72**, 205-212.

Gudehus G., Kolymbas D. 1979. A constitutive law of the rate type for soils. Proc. 3rd Int. Conf. on Num. Meth. Geomech., Aachen (Germany), 319-329.

Hirt C.W., Amsden A.A., Cook J.L. 1974. An arbitrary lagrangian-eulerian computing method for all flow speeds, *Journal for Computational Physics*, **14**, 227-253.

Knupp P.M. 1999. Winslow smoothing on two-dimensional unstructured meshes, *Engineering with Computers*, **15**(3), 263-268.

Marsden J.E., Hughes T.J.R. 1994. *Mathematical Foundations of Elasticity*, Dover Publications, New York (USA).

Nazem M., Sheng D., Carter J.P., Sloan S.W. 2007. Arbitrary lagrangian–eulerian method for large-strain consolidation problems, *International Journal for Numerical and Analytical Methods in Geomechanics*, (to be published).

Niemunis A., Herle I. 1997. Hypoplastic model for cohesionless soils with elastic strain range, *Mechanics of Cohesive-Frictional Materials*, **2**(4), 279-299.

Rodríguez-Ferran A., Casadei F., Huerta A. 1998. ALE stress update for transient and quasistatic processes, *International Journal for Numerical Methods in Engineering*, **43**(2), 241-262.

Savidis S.A., Mittag J. 1999. Vibration measurements in deep excavation pits in Berlin. Proc. Civil and Environ. Eng. Conf., Bangkok (Thailand), II~49-II~54.

Savidis S.A., Aubram D., Li X.-S., Rackwitz F. 2007. Numerical modelling of non-linear soil behaviour under seismic loading conditions, *Soil Dynamics and Earthquake Engineering*, (submitted).

Triantafyllidis T. 1998. Neue Erkenntnisse aus Messungen an tiefen Baugruben am Potsdamer Platz in Berlin, *Bautechnik*, **75**(3), 133-154, (in German).

Truesdell C., Noll W. 2004. *The Non-Linear Field Theories of Mechanics*, 3rd edition, Springer-Verlag, Berlin Heidelberg New York (Germany).